European Review for Medical and Pharmacological Sciences 2022; 26: 5014-5032

Prognosis, immunotherapy and drug therapy of oxidative stress-related genes in patients with hepatocellular carcinoma

S.-S. XIONG

Departments of Pharmacology, School of Pharmacy, Qingdao University Medical College, Qingdao, China

Abstract. – OBJECTIVE: Hepatocellular carcinoma (HCC) is the leading cause of cancer-related death, with high morbidity and low survival. Research on the relationship between cancer cells and oxidative stress has rapidly increased in recent years. Therefore, finding new therapeutic and prognostic targets for hepatocellular carcinoma based on oxidative stress-related genes (OSRGs) has far-reaching significance.

MATERIALS AND METHODS: We first obtained OSRGs on GeneCards and then, based on the TCGA database, compared tumor tissues with normal tissues. Using the LASSO Cox regression method, we obtained six differentially expressed genes associated with prognosis. We also divided all HCC patients in the TCGA cohort into a low-risk group and a high-risk group based on these six genes and accordingly performed a correlation analysis of differentially expressed oxidative-stress-related genes (DEOSRGs). These analyses included GSEA, PPI, survival analysis, immune correlation analysis, tumor microenvironment correlation analysis, m6A analysis, gene mutation analysis, drug-sensitivity analysis, and molecular docking validation. The reliability of the model genes was further verified using a multi-platform database, qRT-PCR and MTT assay.

RESULTS: These six genes may play an important role in the prognosis of hepatocellular carcinoma patients by affecting the kinase, carboxylic acid synthesis and metabolism, ROS production, lipid oxidation and immune response. Validation experiment results further confirm that these model genes are good indicators for the diagnosis and prognosis of hepatocellular carcinoma.

CONCLUSIONS: This study analyzed the prognosis and function of HCC prognosis-related differential genes, predicted that the prognosis-related differential genes played an essential role in HCC immunity, and proposed therapeutic targets and biomarkers for HCC.

Key Words:

Hepatocellular carcinoma, Biomarkers, Oxidative stress, Prognosis, Immune infiltration, Molecular docking.

Abbreviations

Hepatocellular carcinoma (HCC); Oxidative stress-related genes (OSRGs); The cancer genome atlas (TCGA); Least absolute shrinkage and selection operator (LASSO); Differentially expressed oxidative stress-related genes (DEOSRGs); Gene Set Enrichment Analysis (GSEA); t-distributed stochastic neighbor embedding (t-SNE); N6-methyladenosine (m6A); Reactive oxygen species (ROS); Alpha-fetoprotein (AFP); Reactive nitrogen species (RNS); Reduced nicotinamide adenine dinucleotide phosphate (NADPH); Receiver operating characteristic (ROC); Principal component analysis (PCA); Kyoto Encyclopedia of Genes and Genomes (KEGG); Gene ontology (GO); The university of alabama at birmingham cancer data analysis portal (UALCAN); Protein protein interaction (PPI); 3-(4,5-dimethyl-2-thiazolyl)-2,5-diphenyl- 2-H-tetrazoli um bromide (MTT); Real-time fluorescent quantitative PCR (qRT-PCR).

Introduction

Hepatocellular carcinoma (HCC) ranks seventh in the world in terms of incidence, has a high mortality rate, and has no effective treatment[1]. Although HCC can be treated with surgery, it often recurs after surgery. HCC develops rapidly and insidiously and usually is not diagnosed until the disease progresses and has advanced in patients. In recent years, new molecularly targeted drugs have provided a new therapeutic approach to treating advanced HCC. Many studies have focused on exploring more effective predictive signals that could better elucidate the factors that influence the prognosis and progression of HCC and provide more evidence for individual molecular therapeutic approaches. Some current diagnostic markers, such as alpha-fetoprotein (AFP), have many unrelated factors that interfere with their expression, which reduces their sensitivity and specificity[2,3]. Therefore, discovering new therapeutic and prognostic models for HCC is of profound significance.

Oxidative stress refers to the excessive accumulation of highly reactive molecules, such as

Corresponding Author: S.-S. Xiong, MD; e-mail: 2019021017@qdu.edu.cn

reactive oxygen species (ROS) and reactive nitrogen species (RNS), in the body when subjected to various harmful stimuli, resulting in an oxidation imbalance and antioxidant balance, leading to physiological and pathological responses from cells and tissues. Various factors, such as radiation, age, infectious diseases, and heat stress, may lead to increased intracellular ROS concentrations, triggering an intracellular oxidative stress responses that can protect or destroy cells[4-7]. Reactive oxygen species (ROS) are oxygen-derived reactive small molecules, including hydrogen peroxide (H_2O_2), superoxide anion (O_2^-), hydroxyl radical (OH), etc. The mitochondrial and reduced nicotinamide adenine dinucleotide phosphate (NADPH) oxidase families are the two major contributors to endogenous ROS[8,9]. The tight regulation of these ROS levels is essential for cellular life[10]. There are higher levels of ROS in cancer cells compared to normal cells. Sustained high levels of ROS can shift the metabolic pattern of cancer cells from aerobic phosphorylation to anaerobic glycolysis to promote oxidative stress in tumors, also known as the Warburg effect[11,12]. In conclusion, intracellular oxidation–reduction homeostasis mainly depends on the generation of ROS and a balance between enzymatic and non-enzymatic antioxidant systems; once this balance is disturbed, it promotes tumorigenesis and progression[13]. Recent studies[14-17] have shown that oxidative stress can inhibit cancer proliferation and metastasis, Therefore, exploring new OSRGs associated with hepatocellular carcinoma will provide some new possibilities for the prognosis and treatment of HCC.

Based on the TCGA database, we analyze this from the direction of OSRGs, and explore the prognosis and function of OSRGs in HCC using bioinformatics techniques. This study offers new directions for the prognosis of HCC, as well as drug-targeted therapy.

Materials and Methods

Reagent

FerriSeltz, G6PDi-1 and 3-(4,5-dimethyl-2-thiazolyl)-2,5-diphenyl- 2-H-tetrazoliumbromide were obtained from Aladdin (Shanghai, China). FerriSeltz and G6PDi-1 were first dissolved in dimethyl sulfoxide (DMSO, Sigma-Aldrich, St. Louis, MO, USA) and then diluted with culture medium. 3-(4,5-dimethyl-2-thiazolyl)-2,5-diphenyl- 2-H-tetrazoliumbromide was dissolved in PBS (Aladdin, Shanghai, China).

Data Acquisition and Processing

We obtained the dataset using the Illumina Hiseq platform in the TCGA database (https://portal.gdc.cancer.gov/repository), including RNA sequencing (RNA-seq) data and the corresponding clinical characteristics of 374 HCC and 50 normal samples. The clinical characteristics of the included patients are presented in the **Supplementary Table I**. Data normalization correction was performed using the fpkm method, selecting a threshold value of |log2FC| >1.0 and an adjusted *p*-value <0.05, while genes with an average expression level of less than 0.5 were eliminated to ensure that significantly expressed genes were used for the next evaluation. R package "limma" was used as a filter method[18].

Acquisition of OSRGs

We extracted 77 OSRGs from GeneCards (https://www.genecards.org), all of which had correlation scores higher than 20, to identify OSRGs. These OSRGs and the HCC expression data extracted from the database were sorted to obtain the OSRGs related to the database samples.

Differential Expression Analysis

Tumor tissues were compared with normal tissues using the limma package, and differential analysis was performed (|Log2FC| >2, adjusted *p*-value <0.05), combined with the previously obtained OSRGs in the TCGA database HCC Expression of samples versus normal samples. On this basis, the differentially expressed heat map, protein interaction network (https://string-db.org/), and co-expression network were obtained. The obtained DEOSRGs were genotyped and validated in the TCGA database of HCC samples and normal samples.

Biological Functions and Pathway Enrichment

We used "clusterProfiler" package to perform ID transformation on the obtained differential genes and perform Gene Ontology and Kyoto Encyclopedia of Genes and Genomes analysis. Then, the "ggplot2", "enrichplot" packages visualized the analysis results[19-21].

Construction and Validation of P rognostic Models

Clustering analysis was first performed to obtain the DEOSRGs associated with prognosis. Then, univariate Cox regression analysis was used to evaluate the correlation between each oxi-

dative stress-related gene and survival status, and DOSRGs with prognostic value were selected. Then, the LASSO Cox regression model was used to further narrow the range of candidate genes, and a prognostic model was established. Finally, six survival-related model genes were screened out, and a model was established for subsequent analysis. After correcting for TCGA expression data, we calculated risk scores. The risk score formula is as follows: Risk score=∑7iXi×Yi (X: coefficient, Y: gene expression level). HCC patients were divided into two groups according to the median risk score for further analysis. Kaplan-Meier analysis was used to compare survival time between the two groups, followed by receiver operating characteristic (ROC) validation, t-SNE analysis, and principal component analysis (PCA).

Independent Prognostic Analysis of Risk Scores

Independent prognostic analyses of the variables of our prognostic model were performed using univariate and multivariate Cox regression models based on clinical information from HCC patients.

Functional Role Analysis of Differential Genes Based on Prognostic Model

Based on the obtained model genes, enriched enrichment pathways were displayed using the "enrichplot" R package.

Immune-Related Analysis and Tumor Microenvironment Analysis

Using the "GSVA" R package, we performed ssGSEA analysis to quantify the level of cellular infiltration and then assessed the immune response of 22 immune cell subtypes using the CIBERSORT method. In addition, we evaluated the differences and expression levels of 13 immune functions and immune checkpoint expression in the two groups. Finally, we assessed the tumor microenvironment and m6A methylation modifications, and compared the results for high- and low-risk groups, to discuss the impact of model genes on immune cells, stromal cells, and methylation.

qRT-PCR

The differences in the expression levels of the two core model genes in HCC and normal liver cells were confirmed by reverse transcription and quantitative real-time PCR. Quantitative PCR was performed on the QuantStudio 3 system (Thermo Fisher Scientific, Waltham, MA, USA) using ChamQ Universal SYBR qPCR Master Mix (Vazyme, China). After normalization, the relative expression of mRNA was calculated using the 2ΔΔCT method. The primer sequences are shown in Table I.

Cell Viability Assay

Cell viability assay was measured using 3-(4,5-dimethyl-2-thiazolyl)-2,5-diphenyl- 2-H-tetrazoli um bromide (MTT) assay. The cytotoxicity of compounds was tested in Hep3B, Huh7 cells. Cells were plated in 96-well plates at a density of 5×10^3 per well. After being incubated overnight, cells were treated with FerriSeltz and G6PDi-1 at 10 μM and incubated for 72 h. Then, 0.5 mg/ml of MTT 50 μL was added to each well and incubated for 4 h. The solution was removed, and 150 μM dimethyl sulfoxide was added to each well. Finally, we measured the absorbance at 490 nm.

Molecular Docking

We obtained the experimental crystal structure of the *PON1* complex (Protein ID: 1V04) from Protein Data Bank. PubChem (https://pubchem.ncbi.nlm.nih.gov/) provided the three-dimensional structure of the drug. The protein's water molecules and ligands were removed, and polar hydrogen atoms and partial charges were added to MOE. The energy of the drug was then minimized. Using the all-atom docking method, the docked ligands continued to attack the pockets on the protein surface until the most stable docking complex was reached. Scoring energy is the average of trials using the London dG scoring function, upgraded with two uncorrelated refinements using the triangle Matcher method. Finally, the 2D map, 3D map, and pocket docking map of the ligand-protein docking were obtained. All other parameters are set to default unless otherwise specified.

Table I. Primer Nucleotide Sequences for Verification of Differentially Expressed mRNAs.

Gene name	Forward primer	Reverse primer
GSR	AGAAATCATCCGTGGCCATGCA	ACCAACAATGACGCTGCGGC
G6PD	TGAGCCAGATAGGCTGGAA	TAACGCAGGCGATGTTGTC

Statistical Analysis

One-way ANOVA was used to compare gene expression levels between normal lung tissue and HCC tissue, while Pearson's chi-square test was used to compare categorical variables. We used the Kaplan-Meier method, Lasso regression, and two-sided log-rank test to compare the survival prognosis of normal liver tissue and HCC tissue. We assessed the independent prognostic value of risk models using univariate and multivariate Cox regression models. We used the Mann-Whitney test to compare immune cell infiltration, immune function activation, and immune checkpoints between different groups. All the statistical analyses were performed using the R software (v4.1.2).

Results

To Identify OSRGs Associated with Hepatocellular Carcinoma

By comparing the differential expression of 77 OSRGs between different tissues from TCGA data, we obtained 59 differentially expressed target genes (p-value <0.01). Protein–protein interaction (PPI) analysis was then performed to explore the interaction between these DEOSRGs. The minimum interaction score required for PPI analysis was set to 0.9 (highest confidence), and the interaction is shown in Figure 1B. The DEOSRG correlation network is shown in Figure 1C.

Validation of Tumor Typing of DEOSRGs in HCC Samples

To further investigate the association between the expression of 59 DEORGs and HCC, we performed a consensus clustering analysis on HCC samples from the TCGA cohort. By comparing the results of changing the clustering variable (k) from 2 to 10, we found that when k takes a value of 2, the intra-group correlation is highest, and the inter-group correlation is low. (Figure 2A). To further verify the accuracy of typing, we used the cancer marker CD274 to analyze the differences between the normal group and the HCC group and between the typing groups (Figure 2C, D). Then we compared 374 HCC patients' gene expression. Spectral and clinical features such as survival status (alive or dead), age (≤65 or >65 years), and TNM stage (stage I-stage IV) were displayed (Figure 2E). In addition, we also combined the clinical data of TCGA to compare the survival curves of the two types, and the results showed that there was a difference (p-value <0.001, Figure 2B).

Enrichment Analysis of DEOSRGs

Fifty-nine differential genes were subjected to function enrichment analysis. GO analysis results showed that the differential genes were mainly related to cellular response to oxidative stress, antioxidant response, cellular response to chemical stress, response to reactive oxygen species, response to nutrient levels, stimulation of hydrogen peroxide, reactive oxygen species, metabolic processes, cellular responses to reactive oxygen species, mitochondrial gene expression, and mitochondrial matrix processes. KEGG analysis results showed that differential genes were mainly associated with neurodegenerative mutations, lipids and atherosclerosis, chemical carcinogenesis of reactive oxygen species, Parkinson's disease, and the process of amyotrophic lateral sclerosis (Figure 3).

Analysis of Prognostic Model and Validation of Prognostic Model Genes Based on TCGA

Establishment of Prognostic Model

Based on 374 HCC samples in the TCGA database, patients were screened for their complete survival information for subsequent analysis. Univariate Cox regression analysis was used for the initial screening of prognostic model genes. Twenty-five genes meeting the pFilter=0.05 criteria were retained for further analysis, among which, 23 genes (*TXN, NQO1, HMOX1, HADHA, G6PD, GSR, CALM1, OSER1, MRPL44, CASP3, ADPRS, POLR1C, G3BP1, MAPK1, OSGIN2, GTPBP3, OXSR1, CRH, CARS2, MAPK8, OGG1, PNPT1, RYR1*) with HRs >1, suggesting risk genes, while the remaining two genes (*PON1, CAT*) had HRs <1, suggesting protection genes (Figure 4A). By performing the least absolute shrinkage and selection operator (LASSO) Cox regression analysis, a prognostic model was constructed according to the optimal λ value (Figure 4B, C). The model was corrected with six genes involved in the construction of the model. The risk score was calculated by the formula as follows: Risk Score = (0.029* *CARS2*) + (0.010* *GSR*) + (0.003* *G6PD*) + (-0.001* *PON1*) + (0.024* *ADPRS*) + (0.007* *OGG1*). The median was calculated using the risk score formula as a reference; 92 patients were assigned to the low-risk group and 92 to the high-risk group. t-SNE and Principal component analysis (PCA) showed that HCC patients were divided into two

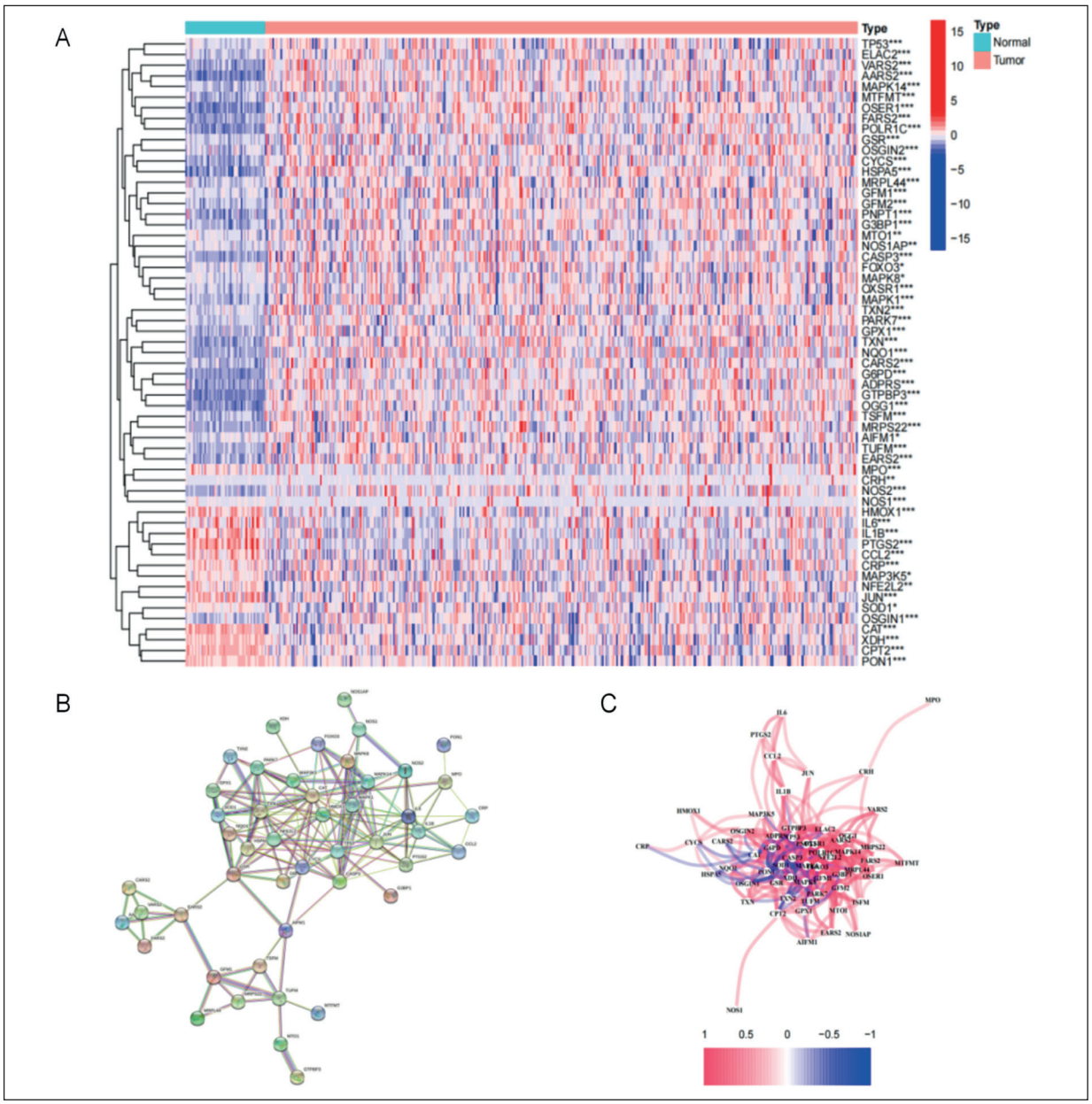

Figure 1. DEOSRGs and their interactions. **A**, DEOSRGs between normal and tumor tissues (blue: low expression level; red: high expression level). **B**, PPI network (taken the highest confidence = 0.9). **C**, Gene correlation network (red line: positive correlation; blue line: negative correlation. Shades of color determined the strength of the correlation). *$p < 0.05$, **$p < 0.001$, ***$p < 0.0001$.

clusters according to the simulated risk score. Patients in the high-risk group had more deaths and shorter survival times than the low-risk group. Performing KM analysis between the low-risk and high-risk groups, we found a significant difference (p-value<0.001). To further evaluate the sensitivity and specificity of the new model, we applied time-dependent ROC and clinical characteristics ROC survival analysis. The areas under the time-dependent ROC curve (AUC) at 1, 3, and 5 years were 0.768, 0.696, and 0.698, indicating significant results (AUC > 0.650, Figure 5A-C).

Validation of the Gene Model in the TCGA Testing Set

In the testing set, 88 patients were assigned to the low-risk group and 95 to the high-risk group. t-SNE and principal component analysis (PCA) showed that HCC patients were divided into two

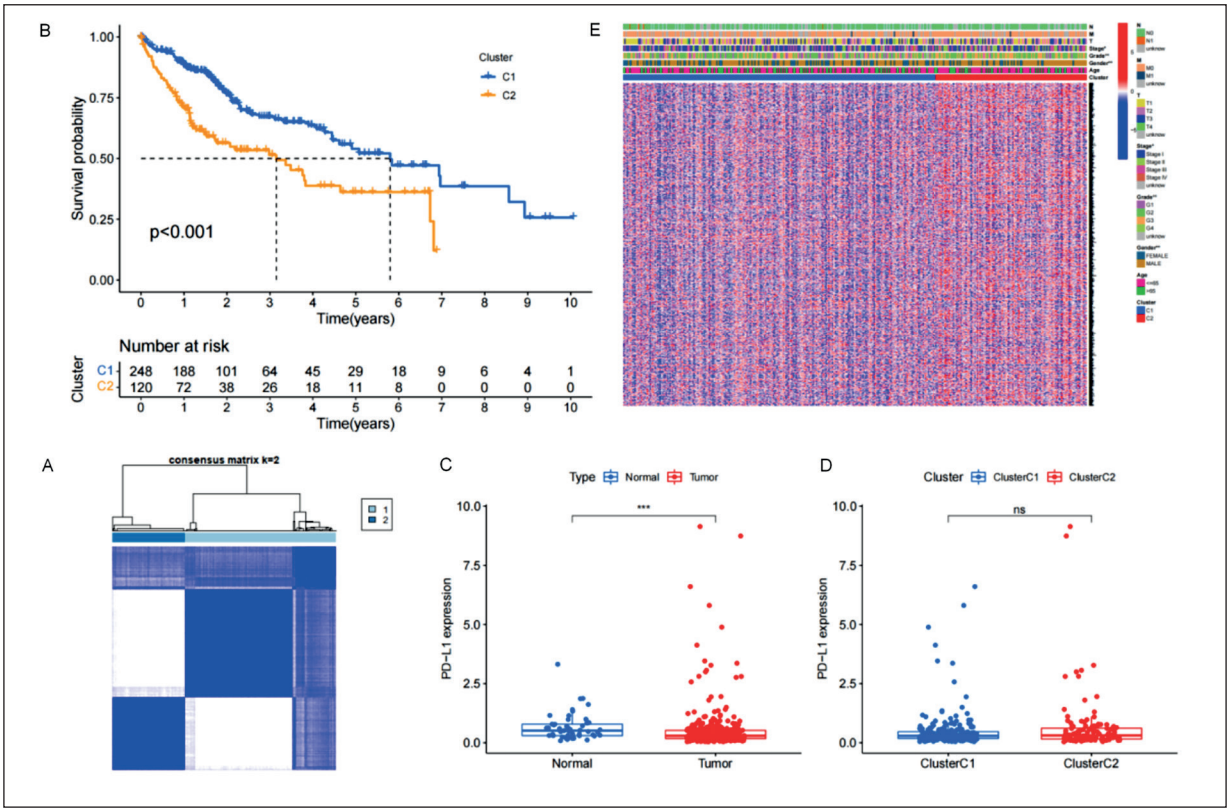

Figure 2. HCC typing based on DEOSRGs. **A**, The 374 HCC patients were divided into two clusters according to the consensus clustering matrix (k = 2). **B**, Kaplan-Meier OS curves of the two clusters. **C**, Difference analysis of the cancer marker CD274 between the normal group and the HCC group. **D**, Difference analysis of the cancer marker CD274 between subgroups. **E**, Heatmap of clinicopathological features of the two clusters of differentially expressed genes. *$p < 0.05$, **$p < 0.001$, ***$p < 0.0001$.

clusters according to the simulated risk score. Patients in the high-risk group had more deaths and shorter survival times than the low-risk group. After performing a KM analysis of the low-risk and high-risk groups, we found a significant difference. The areas under the ROC curve (AUC) at 1, 3, and 5 years were 0.767, 0.675, and 0.605 (Figure 5B-D).

Independent Prediction of Prognostic Model

In the previous section, we obtained a prognostic model. To verify the availability of the prognostic model, we used Cox regression analysis to evaluate whether the risk score of the prognostic model constructed from prognostic related DEOSRGs could be used as an independent prognostic factor. Univariate Cox regression analysis showed that age, risk score, and stage were independent factors for poor survival (p-value <0.05, Figure 6A). These three independent factors were further subjected to multivariate analysis, and the results showed that risk score was an independent factor for poor survival (p-value <0.001, Hazard ratio=1.487, Figure 6B). In addition, we generated a heatmap of clinical characteristics for HCC patients (Figure 6C).

Gene Enrichment Analysis and Clinical Characteristics Correlations of Different Risk Subgroup

We used GSEA analysis to compare gene expression between different groups based on the prognostic model. The KEGG pathway enrichment results revealed that apoptosis-related cell adhesion molecules cam, cytokine receptor interactions, Ecm-receptor interactions, hematopoietic cell lines, and Leishmania infection were significantly increased in high-risk HCC patients. In contrast, multiple cancer-related functions such as drug metabolism cytochrome P450, fatty acid metabolism, glycine serine, threonine metabolism, primary gallbladder acid biosynthesis, and retinol metabolism were up-regulated in the low-risk group (Figure 7A). GO pathway enrichment results showed that immune responses were up-regulated

Figure 3. Bar and bubble charts of GO and KEGG enrichment (longer bars and larger bubbles indicated more gene enrichment).

in the high-risk group, while drug- and fatty acid-metabolism-related functions were up-regulated in the low-risk group (Figure 7B). Then, we investigated the relation of different risk subgroups with clinical characteristics, in which Grade, stage and T were statistically significant (Figure 7C).

Immune-Related Analysis

For immune-related analysis, based on enrichment analysis (ssGSEA), we further compared immune cell correlations and immune-related pathway immune checkpoints between different groups. In the analysis of immune cell infiltration

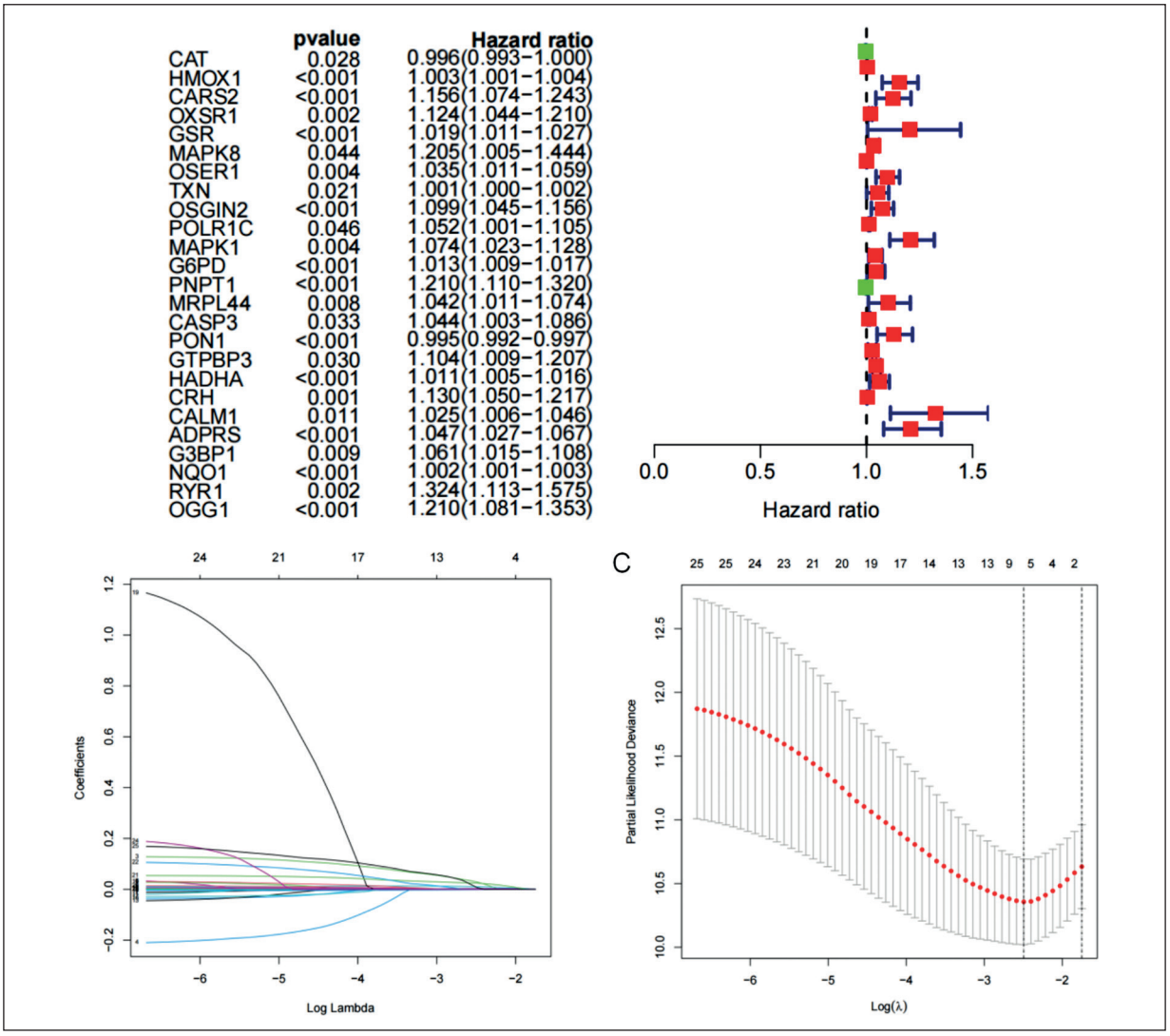

Figure 4. Screening of genes in model construction. **A**, Univariate cox regression analysis. **B**, LASSO regression of DEOSRGs. **C**, Cross-validation of parameter selection in LASSO regression. *$p < 0.05$, **$p < 0.001$, ***$p < 0.0001$.

in different groups combined with the simulation analysis results of different platforms (Figure 8A), we found that the immune cell infiltration response of novel oxidative stress-related gene models was significantly upregulated in HCC. In the analysis of immune-related functions, we found that the expression of immune-related functions in the high-risk group was higher than that in the low-risk group, except for Type_I_IFN_Reponse and Type_II_IFN_Reponse. This indicates that inhibiting the production and release of interferon I and II is one of the leading causes of hepatocarcinogenesis (Figure 8B). Considering the importance of checkpoint inhibitor-based immunotherapy for HCC, a differential analysis of immune checkpoints in different groups was conducted. The expression of all checkpoints in the high-risk group was higher, and the differences were significant (Figure 8C). By analyzing the effect of oxidative stress-related gene models on m6a-related modifications, the methylation expression levels of *METTL3, FTO, YTHDF1, YTHDF2, RBM15, WTAP, YTHDC1, YTHDF2, ALKBH5* and *HNRNPC* were found to be higher in the high-risk group (Figure 8D). Through tumor microenvironment correlation analysis, a significant correlation can be seen between the content of immune cells and stromal cells and the patient's risk score (Figure 8E). Finally, the results of a stem cell correlation analysis showed

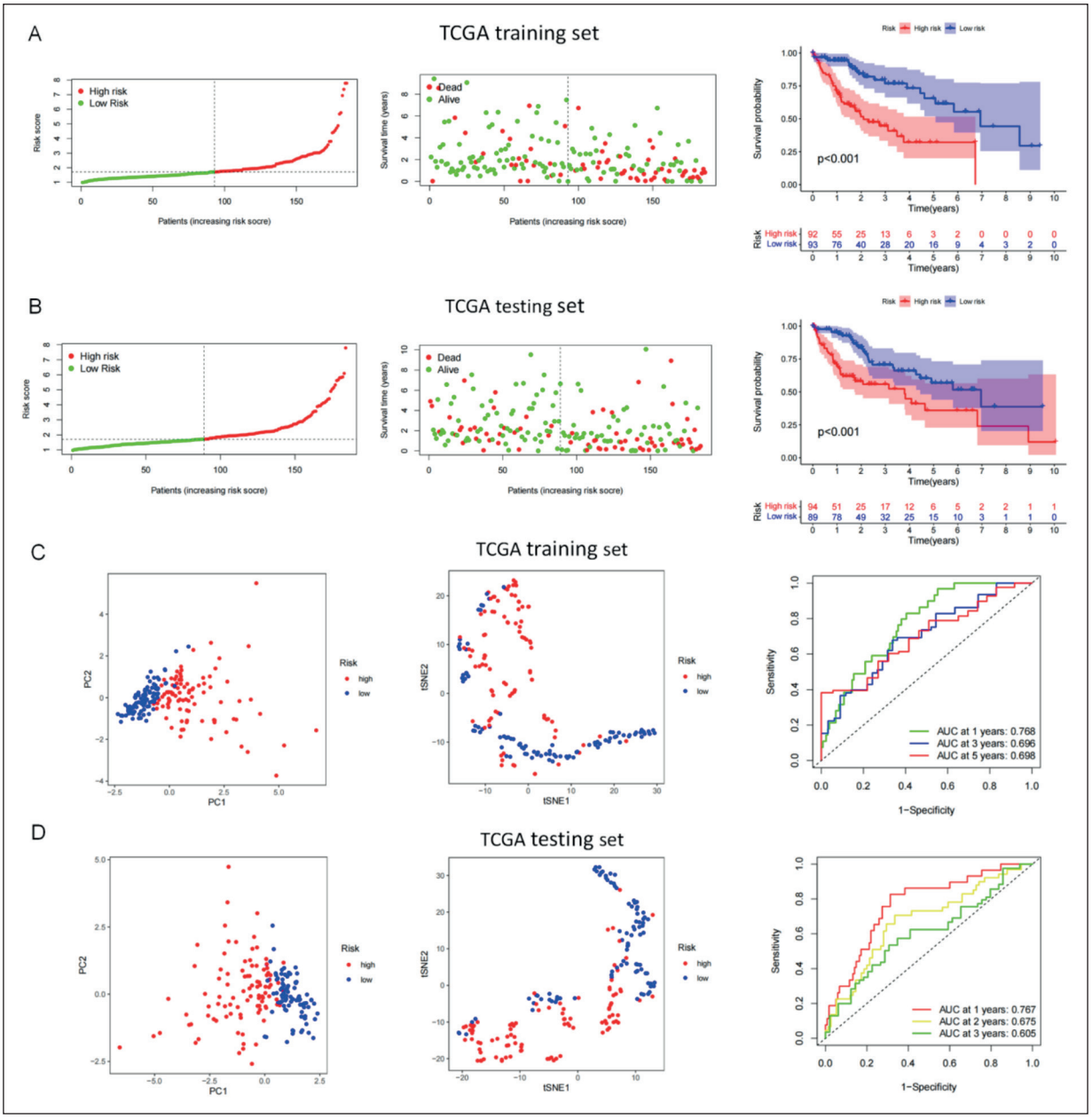

Figure 5. Build self-validated risk prediction model. **A**, 185 patients in TCGA cohort were included in the training set (**B**) 184 patients in TCGA cohort were included in the validation set (**C-D**) ROC, t-SNE, PCA analysis was performed on patients with different risk levels.

that RNA stem cells were significantly correlated with risk scores, while DNA stem cells had no correlation with risk scores (Figure 8F).

Validation of the Role of Model Genes in Hepatocellular Carcinoma

The expression levels of six genes in HCC and paired adjacent normal tissues were compared to explore the clinical significance of this feature. To investigate the protein expression of model genes, we investigated the immunohistochemical results of these six differential genes in normal liver tissue and tumor tissue using the Human Protein Atlas database (https://www.proteinatlas.org/). The results showed that the expression of these six genes was significantly different in the two tissues (Figure 9B). To investigate the mRNA expression of model genes, we used the UALCAN tool (http://ualcan.path.uab.edu/) to study their mRNA expression levels and found that *CARS2,*

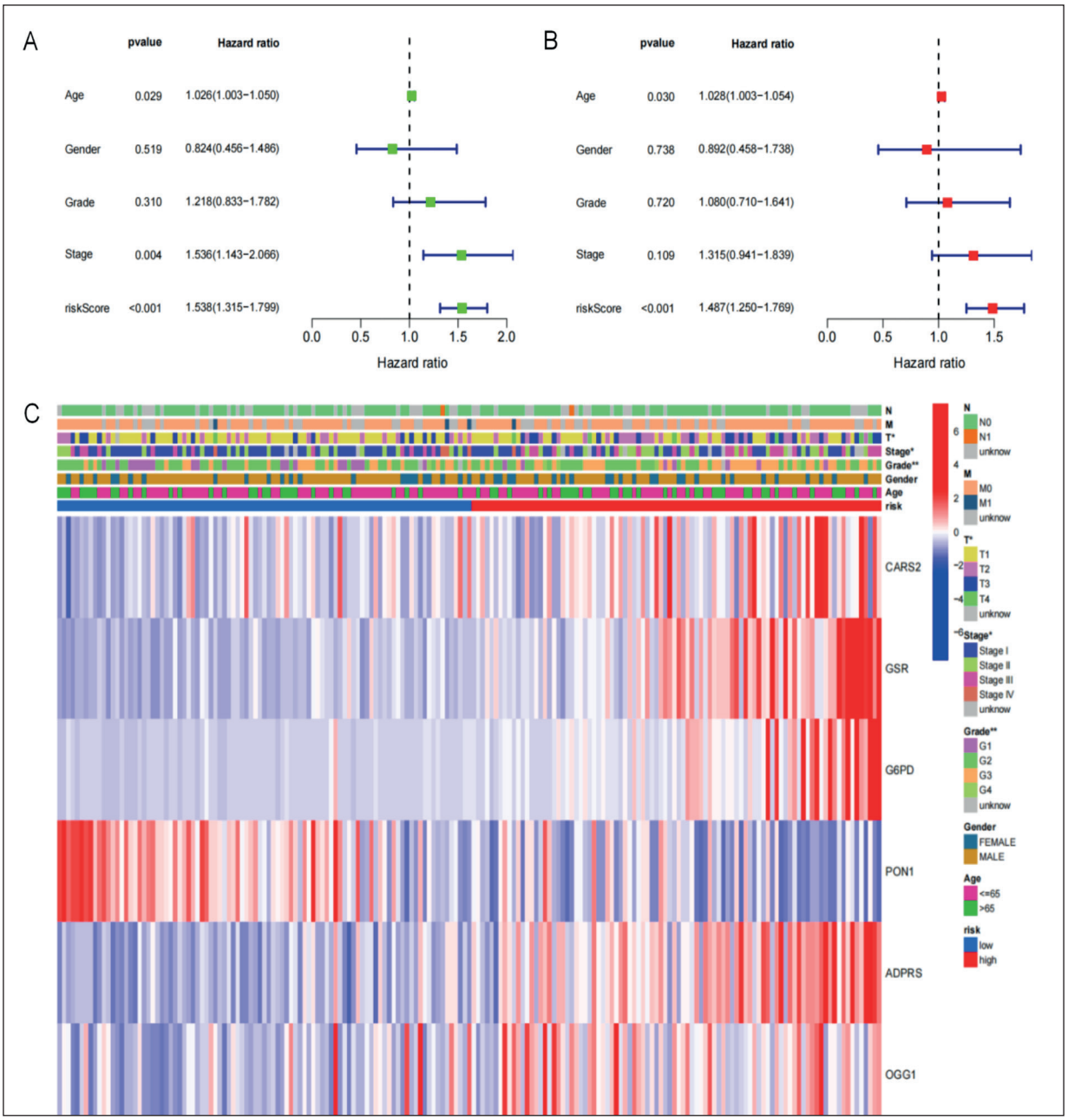

Figure 6. Univariate and multivariate Cox regression analysis to evaluate the clinical prognostic value of the signature. **A**, Univariate analysis. **B**, Multivariate analysis. **C**, Heat map of associations between clinicopathological features and risk groups. *$p < 0.05$, **$p < 0.001$, ***$p < 0.0001$.

GSR, G6PD, ADPRS, OGG1 were up-regulated, while *PON1* was down-regulated (Figure 9A). Next, we constructed a PPI network from the six model risk genes using the String database. Figure 9C shows that *GSR* and *G6PD* are at the center of the network, suggesting that these genes may be the core genes in oxidative stress-related risk models. Therefore, we used real-time quantitative PCR technology to confirm the expression levels of these two key genes in HCC and human normal hepatocytes. As shown in Figure 9D, the expression levels of *GSR* and *G6PD* were higher in HCC than in normal hepatocytes LO2. We verified the biological functions of *GSR* and *G6PD* in hepatocellular carcinoma by further *in vitro* experiments. The proliferation ability of cells was evaluated by MTT assay. The use of FerriSeltz (*GSR* inhibitors) and G6PDi-1 (*G6PD* inhibitors)

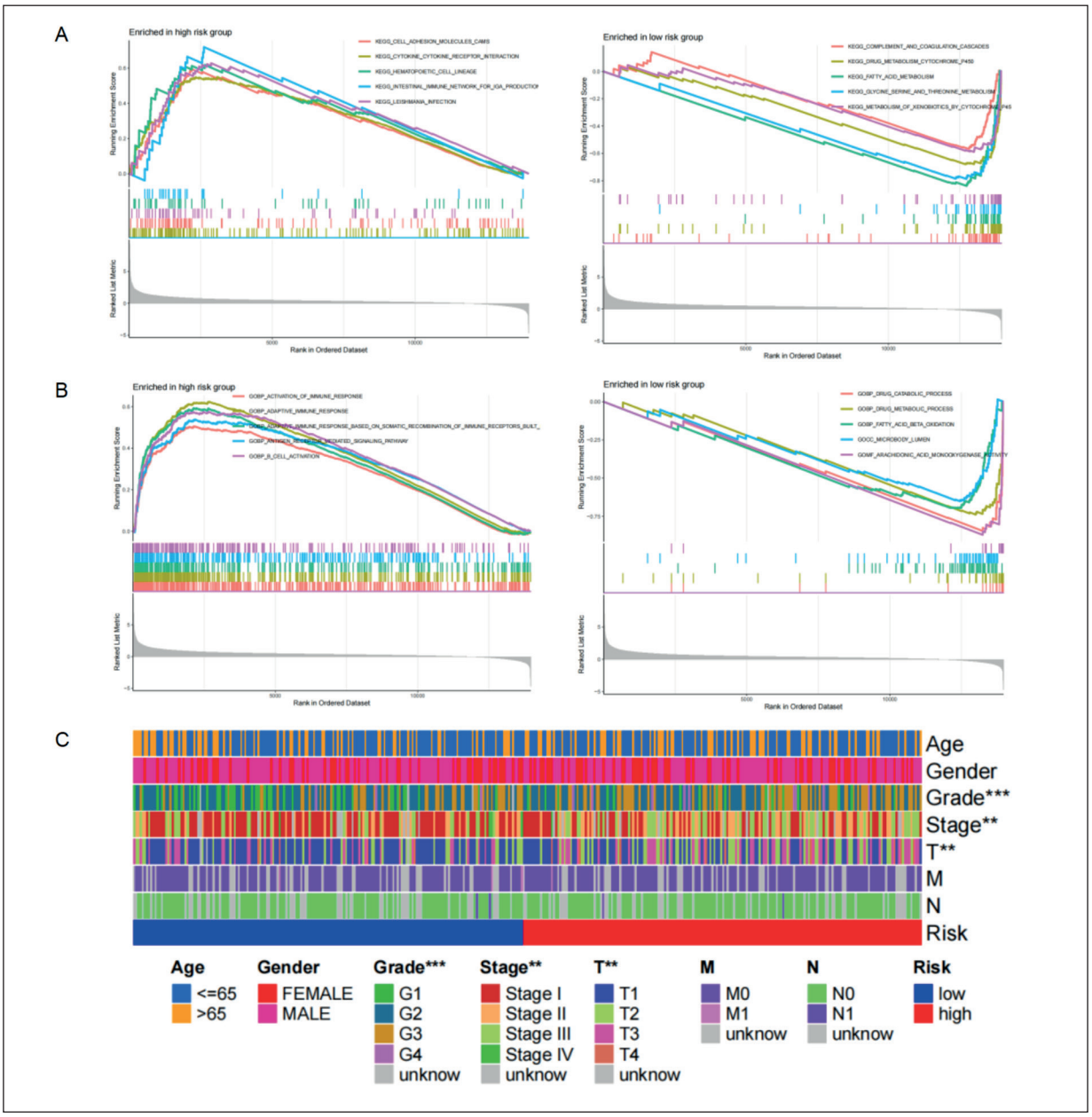

Figure 7. Gene enrichment analysis and clinical characteristics correlations of different risk subgroup. **A**, KEGG pathway. **B**, GO pathway. **C**, Correlation analysis of different clinical features and risk subgroup. *$p < 0.05$, **$p < 0.001$, ***$p < 0.0001$.

inhibited the proliferation of Huh7 and Hep3B cells (Figure 9E.F). Therefore, we determined that *GSR* and *G6PD* function as oncogenes in hepatocellular carcinoma, again showing that oxidative stress model genes are closely related to the progression of hepatocellular carcinoma.

Analysis of Gene Mutation Results

To further understand the genetic characteristics of differential gene, mutation analysis was performed using the cBioPortal database (https://www.cbioportal.org/). *TP53* had the highest mutation frequency (Figure 10A) among the different risk subgroups. The mutation evaluation rates of these six differential genes were all at low levels (Figure 10B).

Drug Sensitivity Analysis

The six model genes associated with prognosis were analyzed with drug sensitivity and transcriptomic data, obtained from the Genomics

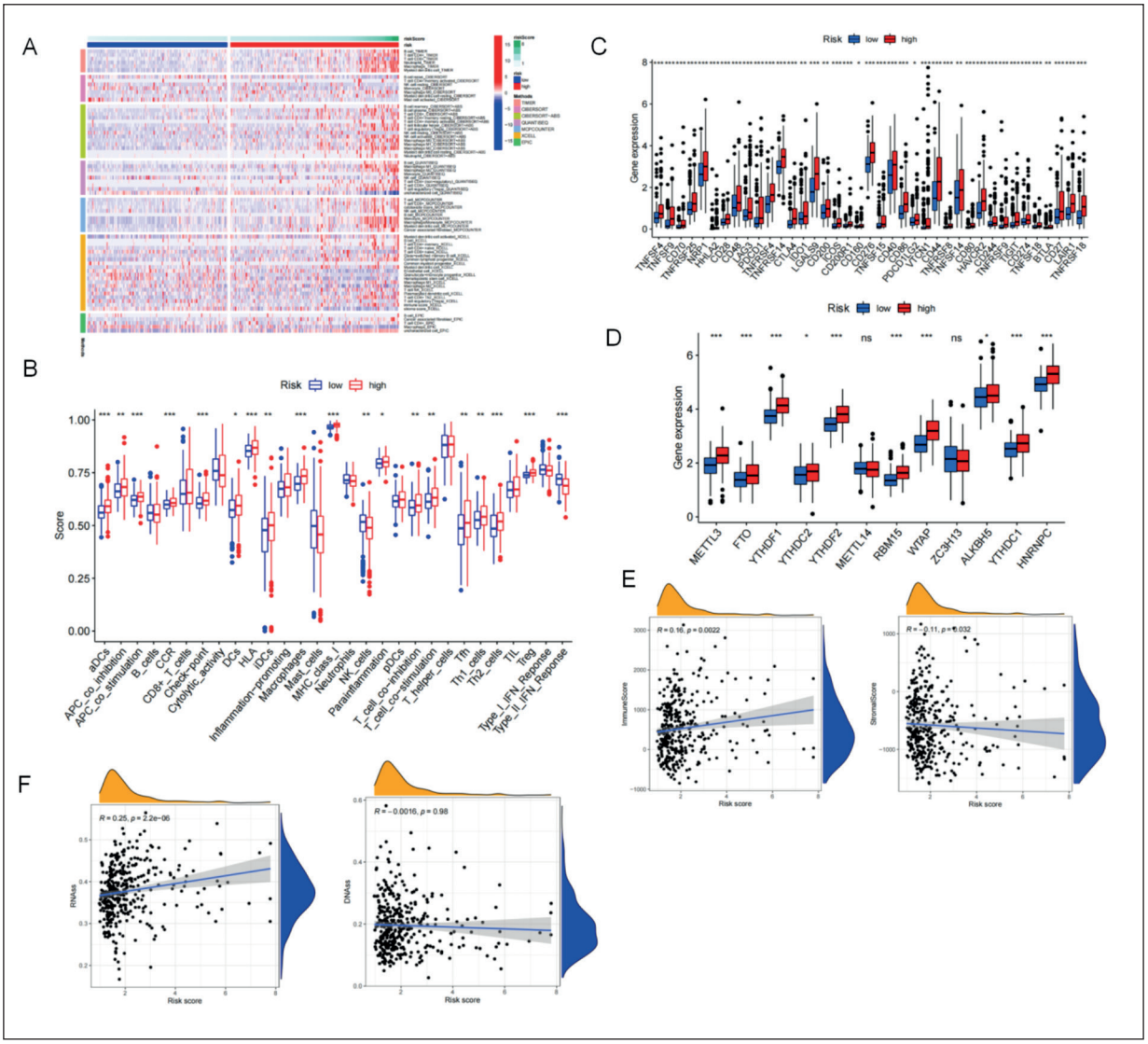

Figure 8. Analysis of immune cells, immune function and immune checkpoints in different risk subgroup. **A**, Immune cell correlation analysis between high-risk groups and low-risk groups. **B**, Immune-related pathway analysis. **C**, Immune checkpoint analysis. **D**, m6A modification expression analysis. **E**, Tumor microenvironment correlation analysis. **F**, Stem cell correlation analysis. $*p < 0.05$, $**p < 0.001$, $***p < 0.0001$.

and Pharmacology Facility (https://discover.nci.nih.gov/). The drug sensitivity analysis of the six model genes and the top 16 drug-related genes were selected for scatter plot drawing (Figure 11).

Molecular Docking Validation Drug Sensitivity Analysis

To further verify the sensitivity analysis results of model genes and drugs, *PON1* (protein ID: 1V04) was selected for molecular docking with four drugs (Asparaginase, Dexamethasone, Fludarabine, Fluphenazine, and Nelarabine). The docking results of *PON1* and the highest-scoring Fluphenazine showed that Fluphenazine was wholly inserted into the active pocket and formed hydrogen bonds at His115, His134, and Asp183, with a minimum binding energy(S) of -7.29 (Figure 12). The docking scoring results showed that the five drugs all matched well with the active region of *PON1*, in line with drug sensitivity results (Table II).

Discussion

In this study, we first investigated the differential expression of 77 OSRGs in HCC and normal

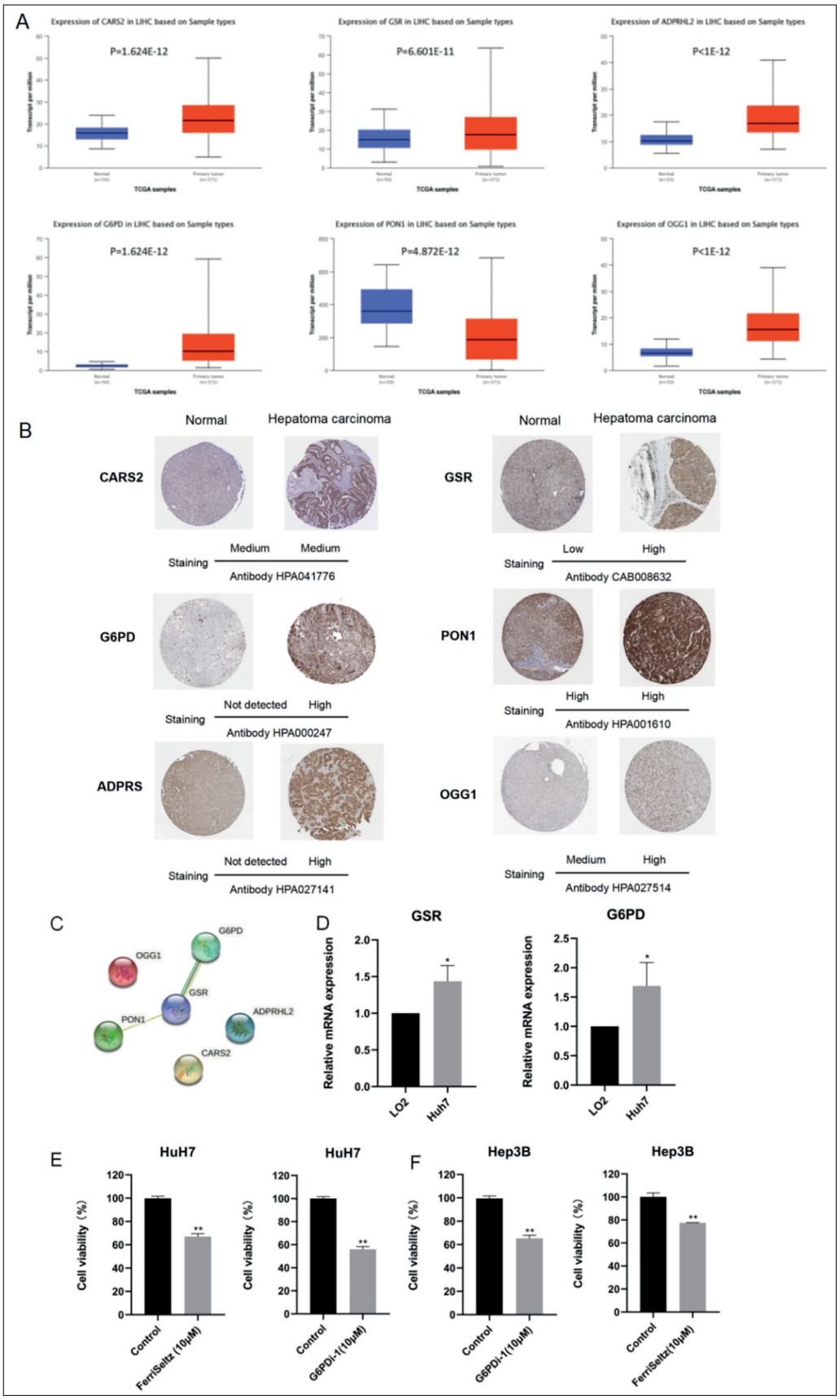

Figure 9. Validation of mRNA and protein expression of model genes. **A**, mRNA expression levels of six model genes in HCC samples and normal samples. **B**, Protein expression levels of six model genes in HCC samples and normal samples. **C**, PPI analysis of model genes. **D**, The differences in the expression levels of the two core model genes in Huh7 cells and LO2 cells. **E**,**F**, Inhibition of GSR and G6PD expression could inhibit the proliferation of Huh7 and Hep3B. *$p < 0.05$, **$p < 0.001$.

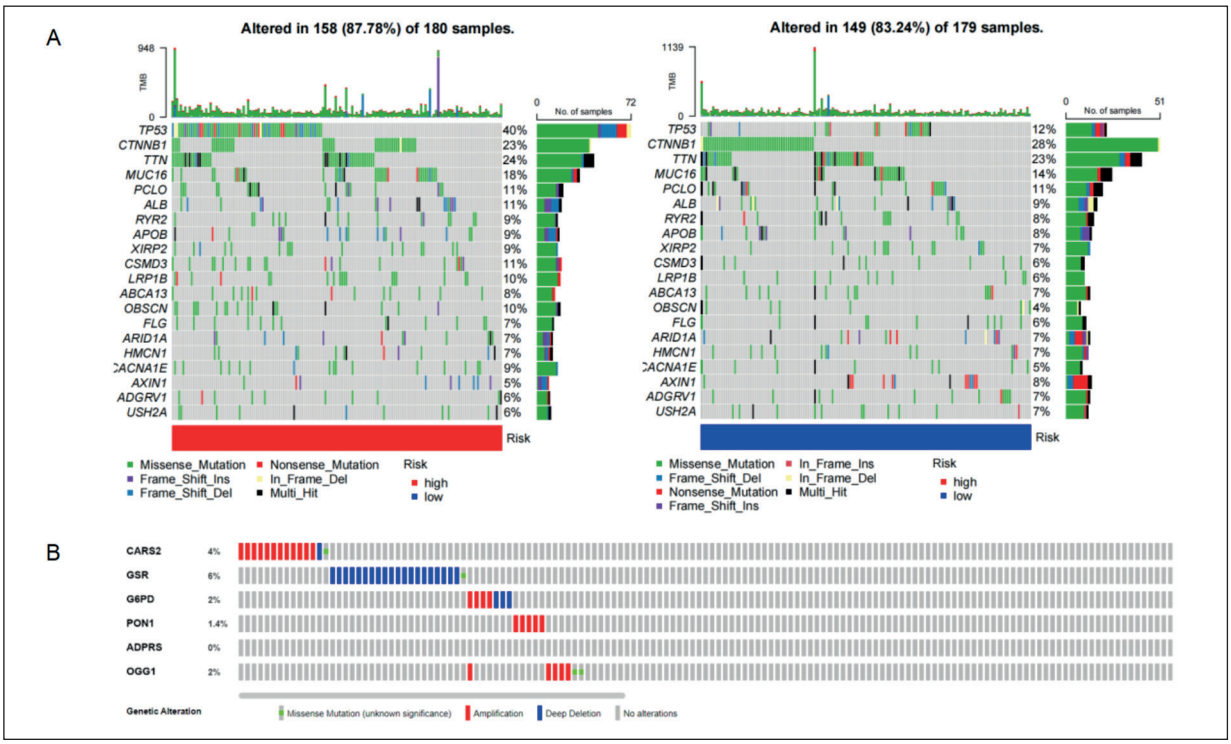

Figure 10. Analysis of gene mutation results. **A**, Mutation frequencies of genes in different risk subgroup. **B**, Genetic variation of model genes.

tissues based on the TCGA database and the GeneCards database, found 59 genes with differential expression associated with prognosis, and investigated their impact on patient overall survival. We then found that the two clusters generated based on a consensus clustering analysis of DEOSRGs differed significantly in terms of their clinical characteristics. To further evaluate the prognostic value of DEOSRGs, we constructed a prognostic model using Cox univariate and multivariate analysis and LASSO Cox regression analysis. Functional analysis showed that antioxidant responses, cellular responses to chemical stress, cellular responses to oxidative stress, responses to reactive oxygen species, responses to nutrient levels, stimulation of hydrogen peroxide, metabolic processes of reactive oxygen species, cellular responses to reactive oxygen species, mitochondrial gene expression, and the mitochondrial matrix were significantly enriched in numerous differentially enriched results. These functions mainly focus on the accumulation of ROS in vivo and may participate in the form of lipid peroxidation caused by ROS. The results of the enrichment analysis were all closely related to the occurrence of HCC, and these relationships were found to be of profound significance for the deeper analysis of these model genes.

Then, we explored these six model genes (*CARS2, GSR, G6PD, PON1, ADPRS, OGG1*) and used them to predict the prognostic model of OS in HCC patients. *CARS2* is a mitochondrial cysteine-specific aminoacyl-tRNA synthetase. Studies have shown that *CARS2* can regulate the metabolism of sulfide and glutathione in cancer cells. Sulfide and glutathione are related to the formation of reactive oxygen species and the sensitivity of cells to ferroptosis caused by the accumulation of reactive oxygen species; therefore, the regulation of *CARS2* may promote tumor ferroptosis[22,23]. However, *CARS2* has not been reported on HCC to date, and is expected to become a new prognostic marker for HCC. *GSR* is a glutathione reductase that forms an integrated network with the antioxidant system of *TrxR1* (thioredoxin reductase-1) and *Nrf2* transcription factors against potentially oncogenic oxidative damage, as well as protecting cancer cells from oxidative death. When *GSR* mutations are inactivated, the level of intracellular oxidative stress increases and the incidence of malignant tumors also increases. This study proves that *GSR* and oxidative stress determine the malignancy of hepatocellular carcinoma[24]. *GSR* is also closely related to the prognosis of hepatocellular carci-

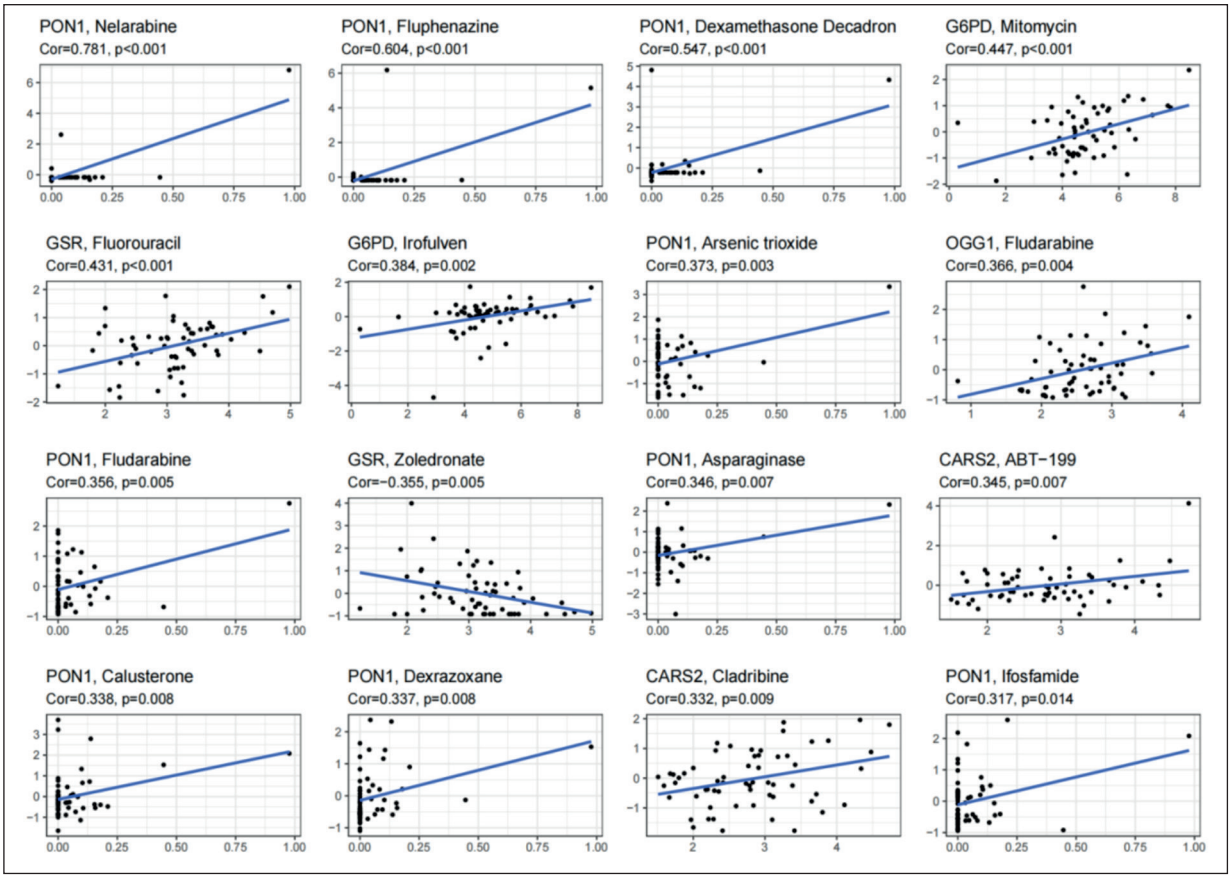

Figure 11. Drug Sensitivity Analysis. Sensitivity analysis of the top 16 pairs of genes and drugs for correlation. *$p < 0.05$, **$p < 0.001$, ***$p < 0.0001$.

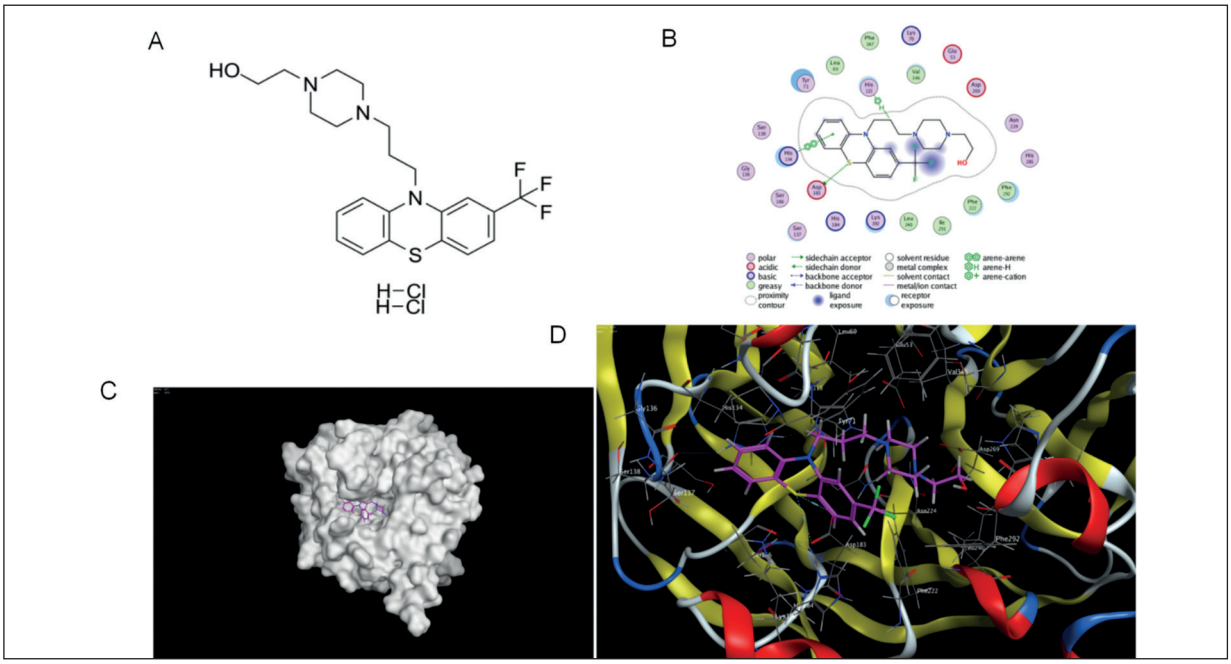

Figure 12. Molecular docking results.**A**, 2D structure of Fluphenazine. **B**, 2D docking diagram of PON1 and Fluphenazine. **C**, Display of the active docking pocket of PON1 and Fluphenazine. **D**, 3D docking diagram of PON1 and Fluphenazine.

Table II. Binding energy of compounds with PON1.

Name	S	rmsd_refine	E_conf	E_place	E_score1	E_refine	E_score2
Asparaginase	-4.361905	1.5004048	-76.84069	-36.11869	-7.854554	-20.03699	-4.361905
Dexamethasone	-6.354526	1.074874	169.44592	-30.55642	-5.635973	-26.72658	-6.354526
Fludarabine	-5.916238	2.1401742	67.819473	-59.29392	-7.632897	-32.57115	-5.916238
Fluphenazine	-7.294916	1.5899478	145.59474	-48.47486	-6.076586	-36.45817	-7.294916
Nelarabine	-5.946387	2.7024329	18.972719	-66.56839	-7.129909	-30.77202	-5.946387

noma. *ADPRS*, an ADP-ribosylserine hydrolase, has been implicated in hormonal status, tumor proliferation, and clinical outcomes[25]. However, there are few studies related to cancer at present, and *ADPRS* is also expected to become a new prognostic marker of HCC. 8-Oxoguanine DNA glycosylase (*OGG1*) is a critical functional protein in the human body. It is an essential protein for oxidative, stress-induced DNA demethylation and plays a crucial role in repairing DNA oxidative damage. Oxidative damage caused by stress can easily lead to inflammatory reactions, and the inhibition of *OGG1* can alleviate this to a certain extent. The inhibition of *OGG1* in cancer cells is expected to be a new method of cancer treatment[26]. Studies have found that it is closely related to the clinical prognosis of thyroid cancer, pancreatic duct adenocarcinoma, leukemia, and lung adenocarcinoma[27-30].Glucose-6-phosphate dehydrogenase (*G6PD*) is the primary regulator of the pentose phosphate pathway and plays an essential role in maintaining the balance of intracellular NADPH and redox reactions. *G6PD* deficiency is the most common hereditary cellular enzyme disease in humans, and previous studies have focused on hemolysis and anemia. In recent years, increasing attention has been paid to the importance of *G6PD* at the cellular level, development, and disease progression. Decreased *G6PD* activity, i.e., the disruption of intracellular redox balance, will lead to the dysregulation of cell growth and signaling, abnormal embryonic development, susceptibility to viruses, and the promotion of degenerative diseases[31-33]. Redox processes lead to oxidative stress in cancer cells and play an essential role in cancer cell growth and development[34-38]. Paraoxonase1 (*PON1*), the full name of aryldialkylphosphatase, is an ester hydrolase present in serum and liver, which catalyzes hydrolysis xenobiotics such as organic phosphorus, unsaturated aliphatic esters, aromatic carboxylic acid esters, carbamates, Etc. The liver is the only synthesis organ of this enzyme[39]. *PON1* can hydrolyze ester bonds to generate hydroxyl radicals (a type of ROS), and the highly accumulated ROS can induce ferroptosis in cancer cells. There have been studies on the correlation between *PON1* and the development of liver, kidney, breast, lung, and colon cancers[40-44], proving that this gene may have important significance for cancer prognosis.

We performed an enrichment analysis of model genes, which showed that apoptosis-related cell adhesion molecules cam, cytokine receptor interactions, Ecm–receptor interactions, hematopoietic cell lines, Leishmania infection, and immune responses were up-regulated in the high-risk group. Mutation analysis showed low mutation frequencies in different risk subgroups, and few mutations in the domains of the six differential genes. To further verify the reliability of model genes, we used the Human Protein Atlas database (https://www.proteinatlas.org/) and the UALCAN tool (http://ualcan.path.uab.edu/) to verify model genes' mRNA and protein expression, respectively. The results showed that *CARS2, GSR, G6PD, ADPRS* and *OGG1* were up-regulated, while *PON1* was down-regulated. Next, we used the string database to perform PPI analysis on six model genes. Using *GSR* and *G6PD* as core genes, we used qRT-RCR to verify that the expression of these two genes in HCC was higher than that in normal hepatocytes, and then used inhibitors to inhibit the expression of these two genes. The results showed that *GSR* and *G6PD* were oncogenes, again proving that the model genes are closely related to the occurrence of hepatocellular carcinoma.

From the perspective of drug analysis, the screened drugs are related to the corresponding target genes and the functions and pathways of enrichment analysis, mainly the production and accumulation of ROS caused by the imbalance of oxidants and antioxidants in the body. In addition, modulating the sensitivity of cancer cells to ferroptosis is the point of action of most drugs. A three-dimensional, longitudinal depth analysis network of target genes, functional pathways, and

drugs was established. Finally, we also performed a molecular docking between the target gene and the corresponding target drug, which theoretically proved the existence of a possible combination of the target gene and the target drug. However, this still needs to be further verified by experiments.

Conclusions

Taken together, based on the DEOSRGs between the normal group and the HCC patient group, the score generated by the risk model of the six model genes is an independent risk factor for predicting overall survival in HCC patients. We believe that these six model genes are closely related to HCC. Combined with the relationship between differentially expressed genes in low-risk and high-risk groups and the immunity and drug sensitivity of HCC, our study provides a new independent prognostic indicator for HCC patients. It also provides a necessary theoretical basis and direction for the immunotherapy and drug treatment of oxidative stress and HCC-related genes in the future.

Conflict of Interest

The Author declares that he has no conflict of interests.

Acknowledgements

We thank the database providing platform used in this article and the contributors who uploaded the dataset.

Data Availability

The datasets and data analyzed in the study are available from the corresponding author on reasonable request.

Ethics Approval and Informed Consent

All the data in this manuscript comes from public datasets, and the corresponding ethical review has been approved by Qingdao University.

References

1) Sung H, Ferlay J, Siegel RL, Laversanne M, Soerjomataram I, Jemal A, Bray F. Global cancer statistics 2020: GLOBOCAN estimates of incidence and mortality worldwide for 36 cancers in 185 countries. CA Cancer J Clin 2021; 71: 209-249.
2) Cai J, Chen L, Zhang Z, Zhang X, Lu X, Liu W, Shi G, Ge Y, Gao P, Yang Y, Ke A, Xiao L, Dong R, Zhu Y, Yang X, Wang J, Zhu T, Yang D, Huang X, Sui C, Qiu S, Shen F, Sun H, Zhou W, Zhou J, Nie J, Zeng C, Stroup EK, Zhang X, Chiu BC-H, Lau WY, He C, Wang H, Zhang W, Fan J. Genome-wide mapping of 5-hydroxymethylcytosines in circulating cell-free DNA as a non-invasive approach for early detection of hepatocellular carcinoma. Gut 2019; 68: 2195-2205.
3) Kim DW, Talati C, Kim R. Hepatocellular carcinoma (HCC): beyond sorafenib-chemotherapy. J Gastrointest Oncol 2017; 8: 256-265.
4) de Sa Junior PL, Dias Camara DA, Porcacchia AS, Moreira Fonseca PM, Jorge SD, Araldi RP, Ferreira AK. The Roles of ROS in Cancer Heterogeneity and Therapy. Oxidative Medicine and Cellular Longevity 2017; 2017: 2467940.
5) Cieslar-Pobuda A, Yue J, Lee HC, Skonieczna M, Wei YH. ROS and Oxidative Stress in Stem Cells. Oxidative Medicine and Cellular Longevity 2017; 2017: 1-2.
6) Tajima M, Sakagami H. Mechanism of endothelial ROS generation by oxidative stress. J Pharmacol Sci 2009; 109: 287P-287P.
7) de Sa PL, Camara DAD, Porcacchia AS, Fonseca PMM, Jorge SD, Araldi RP, Ferreira AK. The Roles of ROS in Cancer Heterogeneity and Therapy. Oxidative Medicine and Cellular Longevity 2017; 2017: 12.
8) Wu B, Li P, Hong X, Xu C, Wang R, Liang Y. The receptor-like cytosolic kinase RIPK activates NADP-malic enzyme 2 to generate NADPH for fueling the ROS production. Mol Plant 2022; S1674205222000867.
9) Sullivan LB, Chandel NS. Mitochondrial reactive oxygen species and cancer. Cancer Metabol 2014; 2: 17.
10) Cheung EC, Vousden KH. The role of ROS in tumour development and progression. Nat Rev Cancer 2022; 22: 280-297.
11) Vo TTT, Vo QC, Tuan VP, Wee Y, Cheng HC, Lee IT. The potentials of carbon monoxide-releasing molecules in cancer treatment: An outlook from ROS biology and medicine. Redox Biol 2021; 46: 102124.
12) Quinlan CL, Treberg JR, Perevoshchikova IV, Orr AL, Brand MD. Native rates of superoxide production from multiple sites in isolated mitochondria measured using endogenous reporters. Free Rad Biol Med 2012; 53: 1807-1817.
13) Costa A, Scholer-Dahirel A, Mechta-Grigoriou F. The role of reactive oxygen species and metabolism on cancer cells and their microenvironment. Semin Cancer Biol 2014; 25: 23-32.
14) Klaunig JE. Oxidative Stress and Cancer. Current Pharmaceutical Design 2018; 24: 4771-4778.
15) Hayes JD, Dinkova-Kostova AT, Tew KD. Oxidative Stress in Cancer. Cancer Cell 2020; 38: 167-197.
16) Jelic MD, Mandic AD, Maricic SM, Srdjenovic BU. Oxidative stress and its role in cancer. J Cancer Res Ther 2021; 17: 22-28.

17) Brugge J. Oxidative stress responses in cancer. Cancer Res 2019; 79: ES6-1-ES6-1.

18) Yuan C, Yuan M, Chen M, Ouyang J, Tan W, Dai F, Yang D, Liu S, Zheng Y, Zhou C, Cheng Y. Prognostic Implication of a Novel Metabolism-Related Gene Signature in Hepatocellular Carcinoma. Front Oncol 2021; 11: 666199.

19) Kanehisa M, Furumichi M, Sato Y, Ishiguro-Watanabe M, Tanabe M. KEGG: integrating viruses and cellular organisms. Nucleic Acids Res 2021; 49: D545-D551.

20) Kanehisa M, Goto S. KEGG: Kyoto Encyclopedia of Genes and Genomes. Nucleic Acids Res 2000; 28: 27-30.

21) Kanehisa M. Toward understanding the origin and evolution of cellular organisms. Protein Sci 2019; 28: 1947-1951.

22) Zheng ZG, Xu H, Suo SS, Xu XL, Ni MW, Gu LH, Chen W, Wang LY, Zhao Y, Tian B, Hua YJ. The Essential Role of H19 Contributing to Cisplatin Resistance by Regulating Glutathione Metabolism in High-Grade Serous Ovarian Cancer. Sci Rep 2016; 6: 26093.

23) Erdelyi K, Ditroi T, Johansson HJ, Czikora A, Balog N, Silwal-Pandit L, Ida T, Olasz J, Hajdu D, Matrai Z, Csuka O, Uchida K, Tovari J, Engebraten O, Akaike T, Dale A-LB, Kasler M, Lehtio J, Nagy P. Reprogrammed transsulfuration promotes basal-like breast tumor progression via realigning cellular cysteine persulfidation. Proc Natl Acad Sci U S A 2021; 118: e2100050118.

24) McLoughlin MR, Orlicky DJ, Prigge JR, Krishna P, Talago EA, Cavigli IR, Eriksson S, Miller CG, Kundert JA, Sayin VI, Sabol RA, Heinemann J, Brandenberger LO, Iverson SV, Bothner B, Papagiannakopoulos T, Shearn CT, Arner ESJ, Schmidt EE. TrxR1, Gsr, and oxidative stress determine hepatocellular carcinoma malignancy. Proc Natl Acad Sci U S A 2019; 116: 11408-11417.

25) Bieche I, Pennaneach V, Driouch K, Vacher S, Zaremba T, Susini A, Lidereau R, Hall J. Variations in the mRNA expression of poly(ADP-ribose) polymerases, poly(ADP-ribose) glycohydrolase and ADP-ribosylhydrolase 3 in breast tumors and impact on clinical outcome. Int J Cancer 2013; 133: 2791-2800.

26) Visnes T, Benitez-Buelga C, Cazares-Korner A, Sanjiv K, Hanna BMF, Mortusewicz O, Rajagopal V, Albers JJ, Hagey DW, Bekkhus T, Eshtad S, Baquero JM, Masuyer G, Wallner O, Muller S, Pham T, Gokturk C, Rasti A, Suman S, Torres-Ruiz R, Sarno A, Wiita E, Homan EJ, Karsten S, Marimuthu K, Michel M, Koolmeister T, Scobie M, Loseva O, Almlof I, Unterlass JE, Pettke A, Bostrom J, Pandey M, Gad H, Herr P, Jemth A-S, El Andaloussi S, Kalderen C, Rodriguez-Perales S, Benitez J, Krokan HE, Altun M, Stenmark P, Berglund UW, Helleday T. Targeting OGG1 arrests cancer cell proliferation by inducing replication stress. Nucleic Acids Res 2020; 48: 12234-12251.

27) Inokuchi S, Itoh S, Yoshizumi T, Yugawa K, Yoshiya S, Toshima T, Takeishi K, Iguchi T, Sanefuji K, Harada N, Sugimachi K, Ikegami T, Kohashi K, Taguchi K, Yonemasu H, Fukuzawa K, Oda Y, Mori M. Mitochondrial expression of the DNA repair enzyme OGG1 improves the prognosis of pancreatic ductal adenocarcinoma. Pancreatology 2020; 20: 1175-1182.

28) Zoraiz K, Attique M, Shahbaz S, Ahmed MW, Kayani MA, Mahjabeen I. Deregulation of mitochondrial sirtuins and OGG1-2a acts as a prognostic and diagnostic biomarker in leukemia. Future Oncol 2021; 17: 3561-3577.

29) Singh A, Singh N, Behera D, Sharma S. Genetic Investigation of Polymorphic OGG1 and MUTYH Genes Towards Increased Susceptibility in Lung Adenocarcinoma and its Impact on Overall Survival of Lung Cancer Patients Treated with Platinum Based Chemotherapy. Pathol Oncol Res 2019; 25: 1327-1340.

30) Zhang Y, He BS, Pan YQ, Xu YQ, Wang SK. Association of OGG1 Ser326Cys polymorphism with colorectal cancer risk: a meta-analysis. Int J Colorectal Dis 2011; 26: 1525-1530.

31) Song J, Sun H, Zhang S, Shan C. The Multiple Roles of Glucose-6-Phosphate Dehydrogenase in Tumorigenesis and Cancer Chemoresistance. Life (Basel) 2022; 12: 271.

32) Jiang J, Jiang Y, Zhang YG, Zhang T, Li JH, Huang DL, Hou J, Tian MY, Sun L, Su XM, Dong Y, Ma YY. The effects of hypoxia on mitochondrial function and metabolism in gastric cancer cells. Transl Cancer Res 2021; 10: 817-826.

33) Zhang Y, Sun S, Xu W, Yang R, Yang Y, Guo J, Ma K, Xu J. Thioredoxin reductase 1 inhibitor shikonin promotes cell necroptosis via SecTRAPs generation and oxygen-coupled redox cycling. Free Radical Biol Med 2022; 180: 52-62.

34) Luo M, Fu A, Wu R, Wei N, Song K, Lim S, Qian K. p High Expression of G6PD Increases Doxorubicin Resistance in Triple Negative Breast Cancer Cells by Maintaining GSH Level. Int J Biol Sci 2022; 18: 1120-1133.

35) Aurora AB, Khivansara V, Leach A, Gill JG, Martin-Sandoval M, Yang C, Kasitinon SY, Bezwada D, Tasdogan A, Gu W, Mathews TP, Zhao Z, DeBerardinis RJ, Morrison SJ. Loss of glucose 6-phosphate dehydrogenase function increases oxidative stress and glutaminolysis in metastasizing melanoma cells. Proc Natl Acad Sci U S A 2022; 119: e2120617119.

36) Kaushik N, Kaushik NK, Choi EH, Kim JH. Blockade of Cellular Energy Metabolism through 6-Aminonicotinamide Reduces Proliferation of Non-Small Lung Cancer Cells by Inducing Endoplasmic Reticulum Stress. Biology (Basel) 2021; 10: 1088.

37) Li Z, He Y, Li Y, Li J, Zhao H, Song G, Miyagishi M, Wu S, Kasim V. NeuroD1 promotes tumor cell proliferation and tumorigenesis by directly activating the pentose phosphate pathway in colorectal carcinoma. Oncogene 2021; 40: 6736-6747.

38) Polat IH, Tarrado-Castellarnau M, Benito A, Hernandez-Carro C, Centelles J, Marin S, Cascante

M. Glutamine Modulates Expression and Function of Glucose 6-Phosphate Dehydrogenase via NRF2 in Colon Cancer Cells. Antioxidants 2021; 10: 1349.

39) Ferre N, Camps J, Prats E, Vilella E, Paul A, Figuera L, Joven J. Serum paraoxonase activity: A new additional test for the improved evaluation of chronic liver damage. Clin Chem 2002; 48: 261-268.

40) Mazzuferi G, Bacchetti T, Islam MO, Ferretti G. High density lipoproteins and oxidative stress in breast cancer. Lipids Health Dis 2021; 20: 143.

41) Pascual-Geler M, Robles-Fernandez I, Monteagudo C, Lopez-Guarnido O, Rodrigo L, Galvez-Ontiveros Y, Cozar JM, Rivas A, Alvarez-Cubero MJ. Impact of oxidative stress SNPs and dietary antioxidant quality score on prostate cancer. Int Food Sci Nutr 2020; 71: 500-508.

42) Aldonza MBD, Son YS, Sung HJ, Ahn JM, Choi YJ, Kim YI, Cho S, Cho JY. Paraoxonase-1 (PON1) induces metastatic potential and apoptosis escape via its antioxidative function in lung cancer cells. Oncotarget 2017; 8: 42817-42835.

43) Ding GY, Zhu XD, Ji Y, Shi GM, Shen YH, Zhou J, Fan J, Sun HC, Huang C. Serum PON1 as a biomarker for the estimation of microvascular invasion in hepatocellular carcinoma. Ann Transl Med 2020; 8: 204.

44) Li X, Yu Q. PON1 hypermethylation is associated with progression of renal cell carcinoma. J Cell Mol Med 2019; 23: 6646-6657.